Translational Oncology
www.transonc.com

Volume 6 Number 6 December 2013 pp. 660–669 660

Effects of Tyrosine Kinase Inhibitors and CXCR4 Antagonist on Tumor Growth and Angiogenesis in Rat Glioma Model: MRI and Protein Analysis Study[1]

Meser M. Ali*,[2], Sanath Kumar†,[2], Adarsh Shankar*, Nadimpalli R. S. Varma*, A. S. M. Iskander*, Branislava Janic*, Wilson B. Chwang*, Rajan Jain*, Abbas Babajeni-Feremi‡, Thaiz F. Borin*, Hassan Bagher-Ebadian*, Stephen L. Brown†, James R. Ewing§ and Ali S. Arbab*,¶

*Cellular and Molecular Imaging Laboratory, Department of Radiology, Henry Ford Hospital, Detroit, MI; †Department of Radiation Oncology, Henry Ford Hospital, Detroit, MI; ‡Division of Clinical Neurosciences, Department of Pediatrics, University of Tennessee Health Science Center, Memphis, TN; §Department of Neurology, Henry Ford Hospital, Detroit, MI; ¶Department of Radiology, Wayne State University School of Medicine, Detroit, MI

Abstract

The aim of the study was to determine the antiangiogenic efficacy of vatalanib, sunitinib, and AMD3100 in an animal model of human glioblastoma (GBM) by using dynamic contrast-enhanced magnetic resonance imaging (DCE-MRI) and tumor protein expression analysis. Orthotopic GBM-bearing animals were randomly assigned either to control group or vatalanib, sunitinib, and AMD3100 treatment groups. Following 2 weeks of drug treatment, tumor growth and vascular parameters were measured using DCE-MRI. Expression of different angiogenic factors in tumor extracts was measured using a membrane-based human antibody array kit. Tumor angiogenesis and invasion were determined by immunohistochemistry. DCE-MRI showed a significant increase in tumor size after vatalanib treatment. AMD3100-treated group showed a significant decrease in a number of vascular parameters determined by DCE-MRI. AMD3100 significantly decreased the expression of different angiogenic factors compared to sunitinib or vatalanib; however, there were no significant changes in vascular density among the groups. Sunitinib-treated animals showed significantly higher migration of the invasive cells, whereas in both vatalanib- and AMD3100-treated animals the invasive cell migration distance was significantly lower compared to that of control. Vatalanib and sunitinib resulted in suboptimal therapeutic effect, but AMD3100 treatment resulted in a significant reduction in tumor growth, permeability, interstitial space volume, and invasion of tumor cells in an animal model of GBM.

Translational Oncology (2013) 6, 660–669

Introduction

Glioblastomas (GBMs) are tumors characterized by hypervascularity and active neovascularization. Various antiangiogenic strategies have been used as adjuvant treatment to normalize blood vessels and control aberrant angiogenesis [1–5]. However, antiangiogenic therapies have been shown to provide only a short-term clinical benefit for about few weeks or months [6–9]. A typical example of such acquired treatment resistance is seen with the use of drugs targeting vascular endothelial growth factor (VEGF) and VEGF receptor (VEGFR) pathway. In our previous work, we observed an increase in the expression of various angiogenic factors, and a significant increase in the number

Address all correspondence to: Ali S. Arbab, MD, PhD, Cellular and Molecular Imaging Laboratory, Department of Radiology, Henry Ford Hospital, 1 Ford Place, 2F, Box-82, Detroit, MI 48202. E-mail: saali@rad.hfh.edu

[1]The work is supported by the National Institutes of Health (NIH) grants R01CA122031 (to A.S.A.), 1R01CA160216 (A.S.A.), 1R01CA172048 (A.S.A.), and K25CA129173 (M.M.A.). The funders had no role in study design, data collection and analysis, decision to publish, or preparation of the manuscript.
[2]Equal contribution.
Received 21 August 2013; Revised 26 September 2013; Accepted 30 September 2013

DOI 10.1593/tlo.13559

of dilated blood vessels following a 2-week treatment with PTK787 (small molecule protein kinase inhibitor that inhibits angiogenesis). Antiangiogenic treatment involves modulation of a wide range of molecular targets [10]. A novel antiangiogenic strategy could be based on the use of broader tyrosine kinase inhibitors that affect not only the VEGFR tyrosine kinase but also other tyrosine kinases as well. One such drug is sunitinib, a small molecule multitarget receptor tyrosine kinase inhibitor, that is known to inhibit signaling through multiple receptors such as platelet-derived growth factor receptors (PDGFRs), VEGFRs, c-KIT, colony-stimulating factor-1 receptor, and fetal liver kinase 3–internal tandem duplication (FLT3-ITD) [11].

Another possible mechanism of antiangiogenic treatment resistance may involve stromal cell–derived factor 1α (SDF-1α) pathway–mediated mobilization of bone marrow (BM)–derived endothelial progenitor cells through CXCR4 receptors on these cells [9,10]. Inhibition of the SDF-1α/CXCR4 axis might prevent the accumulation of endothelial progenitor cells at the tumor site and potentially block vasculogenesis. AMD3100, a potent CXCR4 receptor antagonist, mobilizes CD34+ hematopoietic stem cells into peripheral circulation [12]. Recent investigations have revealed that a continuous treatment with AMD3100 or similar CXCR4 receptor antagonist blocks vasculogenesis, leading to growth inhibition [12,13].

Currently, the efficacy of antiangiogenic therapy is being studied using invasive techniques. The use of noninvasive techniques that allow monitoring of dynamic changes in the tumors after the treatment would allow for better understanding of treatment efficacy and may be more valuable in effectively modifying treatment strategies. Magnetic resonance imaging (MRI) is one of the noninvasive imaging modalities that can be used to monitor dynamic changes in tumors during treatments and subgroup of glioma [14]. Many preclinical and clinical studies have shown that dynamic contrast-enhanced MRI (DCE-MRI) can be useful in assessing tumor vascular parameters and in predicting tumor angiogenesis and tumor response following antiangiogenic therapy [15,16]. DCE-MRI technique measures the pharmacokinetic uptake and washout of an MRI contrast agent within the intracellular and extracellular spaces of tumor tissues, and it can be used to evaluate the vascular forward permeability transfer constant (K^{trans}), backflow transfer constant (K_b), plasma volume of tumor blood volume (V_p), and interstitial space volume (V_e). These parameters have been shown to correlate with tumor perfusion and angiogenesis [17,18].

The purpose of the study was to determine the effects of antiangiogenic treatment on tumor growth in a U251 animal model using vatalanib, sunitinib, and AMD3100 by using DCE-MRI vascular parameters and changes in protein expression.

Materials and Methods

Ethics Statement

Animal experiments were performed according to the NIH guidelines, and the experimental protocol was approved by the Institutional Animal Care and Use Committee of the Henry Ford Health System.

Animal Model

Thirty nude rats (RNU nu/nu), 6 to 8 weeks of age and 150 to 170 g of weight (Charles River Laboratories, Inc, Frederick, MD), were included in the study. Orthotopic glioma was created by injecting 4×10^5 U251 cells suspended in 5 μl of saline at 3 mm to the right and 1 mm anterior to the bregma as described in our previous publications [10,19,20].

Treatment Schedules

Animals were randomly assigned to either the drug treatment (vatalanib, $n = 5$; sunitinib, $n = 8$; and AMD3100, $n = 7$) or the control group ($n = 10$). The control group was treated with the vehicle [cremophor EL/DMSO/phosphate-buffered saline (PBS) at 1:1:8] either by oral gavage ($n = 5$) or by intraperitoneal injection ($n = 5$). Vatalanib (LC Laboratories, Woburn, MA) was prepared for oral administration using the vehicle (cremophor EL/DMSO/PBS at 1:1:8) and was administered orally by gavage, once a day at a dose of 50 mg/kg per feeding for 2 weeks. Sunitinib (LC Laboratories) was dissolved in the vehicle and administered by intraperitoneal injection at a dose of 80 mg/kg per day for 2 weeks. AMD3100 (TORCIS Bioscience, Minneapolis, MN) was dissolved in distilled water and injected subcutaneously at a dose of 5 mg/kg per day (divided into two doses per day) for 2 weeks. Drug administration started 8 days after tumor implantation and continued for two weeks (5 days/week). Twenty-two days after tumor implantation, animals underwent *in vivo* DCE-MRI followed by euthanasia and collection of brain tissue.

In Vivo *MRI*

Animals were anesthetized with 2% isoflurane in oxygen carrier gas and secured to a customized cradle. A 26-g dental catheter was inserted into a tail vein to facilitate the injection of contrast agents. The animal body temperature was maintained at 37.0°C during scan within the MRI magnet. MRIs were obtained with a 3T clinical system (Signa Excite; GE Healthcare, Wauwatosa, WI) using 50 mm × 108 mm RF rung length small animal imaging coil (Litzcage small animal imaging system; Doty Scientific Inc, Columbia, SC). Precontrast and postcontrast T1-weighted images (T1WIs), multiecho T2-weighted images (T2WIs), and three-dimensional spoiled gradient echo (3D SPGR) images of the tumor-bearing brain were acquired before (four to five sequences) and sequentially up to 20 minutes following IV injection of gadolinium-diethylenetriamine pentaacitic acid (Gd-DTPA). The following parameters were used to acquire the images. For T1WIs, repetition time (TR) = 625 ms, echo time (TE) = 15 ms using a 160 × 128 matrix, field of view (FOV) = 35 mm, and number of excitation (NEX) = 4; effective slice thickness was 1 mm, and 15 slices were imaged. For multiecho T2WIs, TR = 2100 ms, TE = 15, 30, 45, and 60 using a 160 × 128 matrix, FOV = 35 mm, and NEX = 2. - Effective slice thickness was 1 mm, and 15 slices were imaged. Multiecho T2WIs were used to create T2 maps. To generate T1 maps from precontrast images, 3D SPGR images with multiple flip angles of 2°, 4°, 8°, 12°, 15°, 20 °, 25 °, 30°, and 35° were acquired. The following parameters were used to acquire the 3D SPGR images: TR = 5.65 ms, TE = 1.35 ms using a 128 × 128 matrix, FOV = 60 × 60 × 18 mm^3, and NEX = 1. Effective slice thickness was 1.5 mm. To obtain dynamic postcontrast 3D SPGR images, a fixed flip angle of 30° was used. Acquisition of SPGR images started before the administration of contrast to have baseline T1 signals.

Kinetic Analysis

DCE-MRI was performed using a transverse T1W 3D SPGR acquisition that consisted of obtaining precontrast (four to five sequences) and dynamic postcontrast images up to 20 minutes after the contrast injection. We used the DCE-MRIs and the following

Patlak model to estimate the transfer constants K^{trans} and K_b, plasma volume of tumor blood volume (V_p), and interstitial space volume (V_e) according to the following equation [17,18]:

$$C_t(t) = K^{trans} \int_0^t C_p(\tau) e^{-K_b(t-\tau)} d\tau + V_p C_p(t).$$

$C_t(t)$ and $C_p(t)$ are the tissue and the plasma concentrations over time, respectively. K^{trans} is the unidirectional transfer rate constant of the contrast from plasma across the vascular endothelium and blood-brain barrier into the interstitial fluid. K_b is the reverse transfer rate constant from the extravascular compartment to the vascular compartment. V_p is the fractional volume of the contrast agent vascular distribution space, usually thought to be the plasma distribution space. If the transvascular transfer of the contrast agent is passive, the two rate constants are related through the interstitial space volume fraction: $V_e = K^{trans}/K_b$. Our recent publication shows the validity of this method [17]. The K^{trans}, K_b, V_p, and V_e of the tumors (both treated and control) were determined by drawing irregular regions of interests (ROIs) encompassing the whole tumor. An investigator blinded to both treated and untreated animals drew the ROIs and determined the values.

Measurement of Tumor Volume

Postcontrast T1WIs were used to determine the volume of the tumor in each animal. Two investigators blinded to the treatment groups determined the volume by drawing irregular ROIs around the tumor and multiplying the area with the slice thickness.

Protein Extraction from Tumors

Animals were killed, and brain tissues were collected after perfusion using ice-cold 1× PBS. The tumor-bearing hemisphere and contralateral brain were separated, snap frozen, and stored at −80°C. On the day of protein extraction, tumor was carefully separated from the surrounding brain tissues and total protein from the tumor was extracted using mechanical pulverization over dry ice and 2× RayBio cell lysis buffer according to the manufacturer's instructions (RayBiotech, Inc, Norcross, GA). Total protein concentration was measured by Bio-Rad Protein Assay (Bio-Rad Laboratories, Hercules, CA) using BSA as a standard.

Protein Analysis

The levels of specific cytokines/factors within the tumor-extracted total protein were analyzed using a custom-designed membrane-based human cytokine antibody array kit from RayBiotech, Inc according to the recommended method of the vendor. The membrane-based quantitative antibody array has a standard membrane spotted with 20 cytokine capture antibodies, and the detection is based on chemiluminescent labeling. Positive signals were detected with chemiluminescent detection solution using Multispectral Imaging System (Carestream, Rochester, NY). Images were analyzed using ImageJ software (NIH). The density of each signal was normalized using positive controls included on the membrane as well as corresponding values in the control animals. The following factors were analyzed: angiogenin, angiostatin, angiopoietin-1, angiopoietin-2, granulocyte colony stimulating factor (G-CSF), PDGF-AA, PDGFR-A, RANTES, basic fibroblast growth factor (bFGF), epidermal growth factor (EGF), EGF receptor, insulin growth factor-1 (IGF-1), matrix metalloproteinase-9 (MMP-9), SDF-1α, Tie-1, Tie-2, VEGF-A, VEGF-C, VEGFR2, and VEGFR3. Table 1 shows the relative characteristics of the growth factors in angiogenesis.

Table 1. Angiogenesis-Related Growth Factors in GBM Tumors.

Growth Factor–Related Angiogenesis	Stimulation	Inhibition
Angiogenin	+	−
Angiostatin	−	+
Angiopoietin	+	−
Tie-1 and Tie-2	+	−
G-CSF	+	−
bFGF	+	−
SDF-1	+	−
RANTES	+	−
VEGF/VEGFR	+	−
PDGF	+	−
EGF	+	−
EGF receptor	+	−
MMP-9	−	+
IGF-1	+	−
MMP-2	+	−
HIF-1α	+	−

Protein Estimation by ELISA

MMP-2 and hypoxia inducible factor-1 (HIF-1α) were quantified as a marker for tumor infiltration and hypoxia, respectively. MMP-2 and HIF-1α levels were determined in the vehicle and drug-treated tumors using ELISA kit according to the manufacturer's instructions (RayBiotech, Inc). All values were normalized to the corresponding values in the control animals.

Histopathology

Animals used for the histologic analysis were killed and perfused by intracardiac injection of 100 ml of PBS, followed by 3% paraformaldehyde. Brains were collected and fixed in 3% paraformaldehyde containing 3% sucrose. Tissue sections were prepared from either frozen or paraffin preparations. Standard histochemical staining procedures were performed as recommended by the suppliers of primary antibodies. Our histochemical analysis concentrated on the markers of neovascularization, invasion, and human-specific cells. Sections were stained to determine neovascularization by using von Willebrand factor (vWF; Dako, Carpinteria, CA) and invasion of tumor cells by targeting human-specific major histocompatibility complex-1 (MHC-1), cluster of differentiation 44 (CD44), and MMP-2 (all antibodies were from Lab Vision, Kalamazoo, MI). CD44-positive cells are considered as highly migratory, tumor stem cell like, and resistant to drug treatments [21–23]. MMP-2 is known for its involvement in a breakdown of extracellular matrix that makes the way for tumor invasion. MHC-1 and MMP-2 were double stained to determine if the migration of human cells (2° IgG + fluorescein isothiocyanate) was related to MMP-2 (2° IgG + rhodamine)–positive areas. Consecutive sections were also double stained with vWF (2° IgG + rhodamine) and CD44 (2° IgG + rhodamine) to determine if the invasive cells migrated at the regions of neovascularization.

Evaluation of Microvessel Density

Microvessels were detected by immunohistochemical staining with vWF. vWF staining is well established for determining neovascularization

in different lesions [24–26]. Each cell positive for vWF was considered to be a microvessel. Five "hot spots" (area with highest vessel concentration) from each slide were identified, and vWF-positive areas were counted by two independent observers. The total area of histologic section viewed on microphotography was noted, and microvessel density (MVD) was calculated as previously described [27].

Tumor Cell Migration and Invasion

The distance between the MHC-1–positive cells and the margin of the primary tumor mass was evaluated using low, ×4 to ×10, image magnification. The tumor periphery was confirmed on high magnification before all measurements. An irregular line was drawn at the most peripheral part of the tumor that showed continuation to the primary tumor mass. Any MHC-1–positive cells away from the drawn line were considered invasive cells away from the primary tumor mass. A perpendicular line was drawn from the invasive tumor cells or tumor foci (center of the foci) to the drawn line at the tumor periphery, and the distance was noted. Distance from migrated individual cell or distal tumor foci to the periphery of the primary tumor mass was determined, and the average values were calculated. The analysis was done using the software supplied by the vendor (ToupView Software, Irvine, CA). The average distance between the MHC-1–positive cells and the tumor margin was determined for vatalanib, sunitinib, AMD3100, and vehicle-treated tumors. Consecutive sections of the tumor were stained to determine the expression of vWF, CD44, and MMP-2 at the corresponding sites of tumor cell invasion.

Statistical Analysis

Comparison between drug and vehicle-treated groups was done by using one-way analysis of variance with protected least significant difference (PLSD) post hoc test. All data are expressed as means ± SEM. Any P value of <.05 was considered significant.

Results

Effects of Vatalanib, Sunitinib, and AMD3100 on Tumor Growth

All animals showed measurable and well-enhanced tumor in the right brain hemisphere by day 22, and all tumors were detected by postcontrast T1WIs (Figure 1*A*). Tumor volumes measured from postcontrast T1WIs are shown in Figure 1*C*. Compared to the control, tumors treated with vatalanib showed significantly increased volume following treatment ($P < .01$). However, both sunitinib and AMD3100 treatments resulted in a nonsignificant decrease in the tumor size, compared to the vehicle treatment ($P = .25$ and $P = .45$, respectively). T2WIs confirmed the changes in the tumor size as seen on T1WIs (Figure 1*B*). However, no significant differences in T2 values were observed between the control and drug-treated groups (Figure 1*D*), indicating the absence of necrosis or edema following drug treatments.

DCE-MRI Vascular Parameter Analysis

The following vascular parameters were estimated using DCE-MRI in vehicle and drug-treated tumors: K^{trans}, K_b, V_p, and V_e (Figure 2).

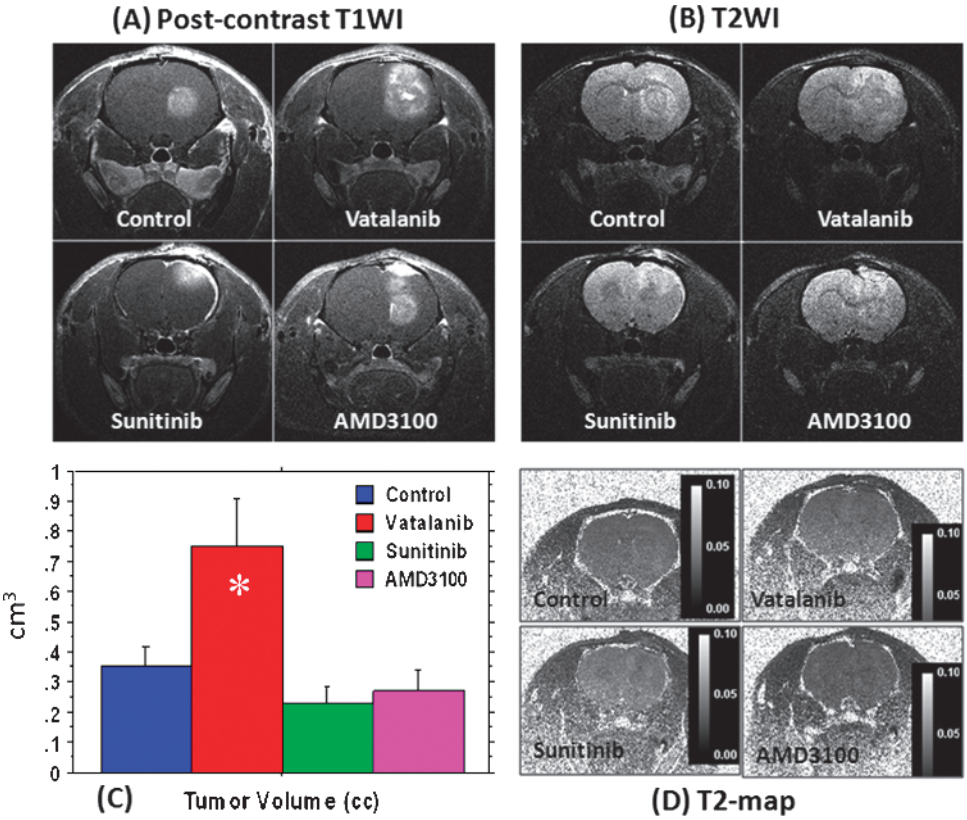

Figure 1. Effect of antiangiogenic treatment in U251 tumor determined by MRI. Postcontrast T1WI (A) and T2WI changes (B) after 2 weeks of antiangiogenic treatment with vatalanib, sunitinib, and AMD3100; tumor volumes measured after vehicle and drug treatment (C); T2 maps of U251 tumors following antiangiogenic therapy showed no significant edema or necrosis compared to the vehicle-treated tumor (D). *$P < .05$. All tumors were in the right hemisphere.

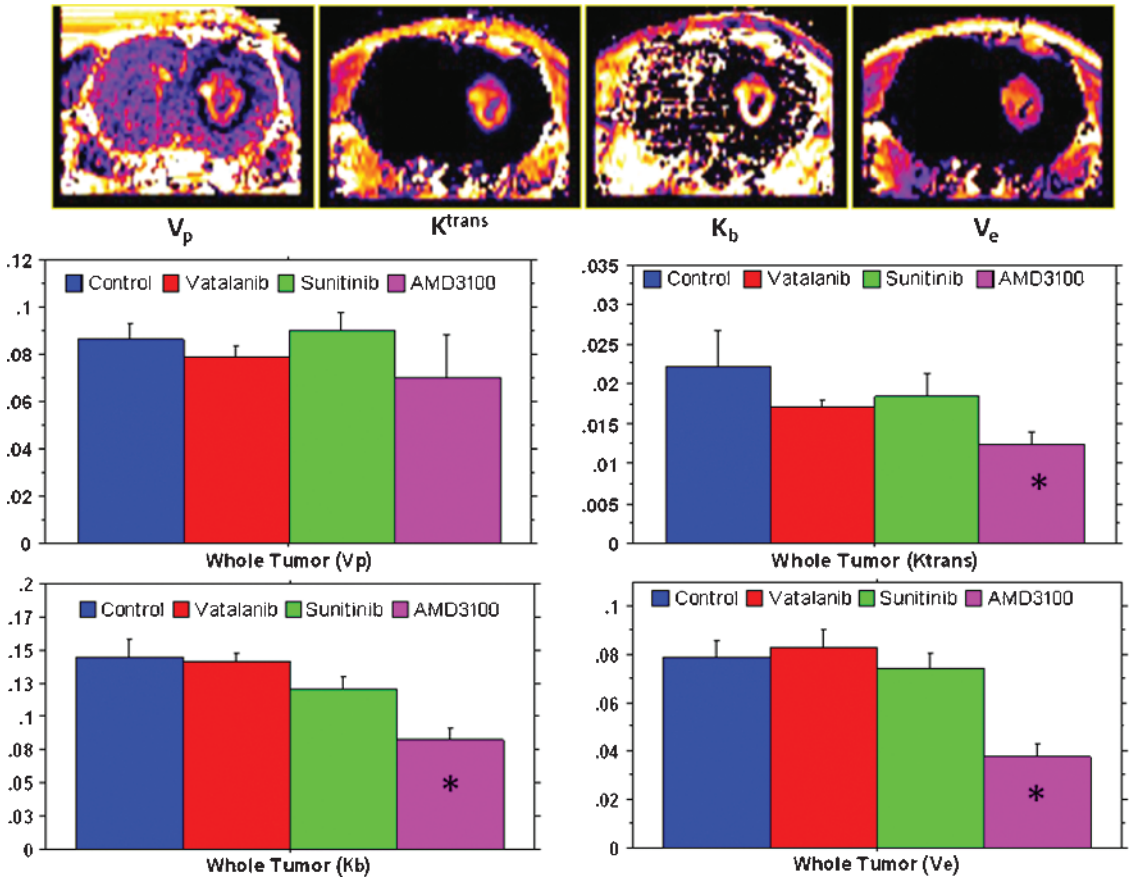

Figure 2. MRI vascular parametric analysis after antiangiogenic therapy. The upper panel shows maps from a representative case showing tumor plasma volume (V_p), vascular forward transfer constant (K^{trans}), backflow transfer constant (K_b), and interstitial space volume (V_e). The middle and lower panels show quantitative estimations of V_p, K^{trans}, K_b, and V_e after the drug treatment. Note the significant decreased K^{trans}, K_b, and V_e in tumors treated with AMD3100. *$P < .05$. All tumors were in the right hemisphere.

There was no significant difference observed for V_p among the groups treated with vatalanib, sunitinib, AMD3100, and vehicle. Vatalanib, sunitinib, and AMD3100 treatments resulted in a decrease in tumor K^{trans} (whole tumor) compared to the vehicle treatment. However, a significant decrease in the K^{trans} value was only observed for the tumors treated with AMD3100 ($P < .01$). Similarly, a decrease in K_b was observed in tumors treated with either vatalanib or sunitinib or AMD3100, compared to vehicle treatment. However, the decrease was only significant for the AMD3100 treatment group ($P < .0001$). V_e was increased after vatalanib treatment compared to vehicle treatment. However, only AMD3100 treatment significantly ($P < .001$) reduced V_e in the tumors compared to the vehicle treatment. The DCE-MRI results indicate that there was a significant decrease in the tumor vascular permeability after AMD3100 treatment, compared to the vehicle treatment. However, vatalanib treatment resulted in a net increase in the tumor volume and interstitial space, as indicated by the increase in V_e compared to vehicle treatment. Compared to the control group, there was no significant change in the tumor growth and vascular parameters after sunitinib treatment. The experiment results indicate that AMD3100-treated tumors showed greater antitumor responses on DCE-MRI, compared to the sunitinib- and vatalanib-treated tumors.

Protein Array

The results are summarized in Figure 3. An increase in the expression of angiostatin, an antiangiogenic protein, was observed in the tumors treated with vatalanib, sunitinib, and AMD3100 compared to vehicle treatment; however, this difference reached the significance in the animals treated with sunitinib. Changes in the expression levels of proangiogenic factors in response to vatalanib, sunitinib, and AMD3100 are shown in Figure 3. AMD3100 treatment resulted in a net decrease in the expression of most proangiogenic factors tested compared to the vehicle treatment, with the significant decrease seen in the expression of IGF-1, VEGFR2, and VEGF-C. Sunitinib treatment resulted in an increase in the expression of proangiogenic growth factors including bFGF, PDGF-AA, EGF, SDF-1, angiopoietin-1 and angiopoietin-2, and Tie-1 and Tie-2, compared to vehicle treatment. Similarly, vatalanib treatment led to an increased expression of various proangiogenic growth factors compared to vehicle treatment. The expression of G-CSF was significantly higher after vatalanib treatment, compared to vehicle treatment, whereas sunitinib and AMD3100 decreased the expression of G-CSF, compared to that of vehicle-treated animals (Figure 3).

Histologic Analysis

Tumor angiogenesis and MVD. Tumor neovascularization was assessed by quantification of MVD. Histologic evaluation of MVD following 2 weeks of treatments showed no significant differences among

different groups of animals treated with either one of the drugs or vehicle (Figure 4).

Tumor cell migration. To identify implanted tumor human origin cells, we have used antibodies specific for human MHC-1 molecule. The distance of the MHC-1–positive cells' location from the primary tumor mass was measured and used as an assessment of tumor invasiveness and the ability of tumor cells to migrate away from the primary tumor. Tumors in the drug treatment group exhibited multiple foci of human cells located away from the margin of the primary tumors. However, on quantitative evaluation, the average distance migrated by the tumor cells was significantly higher in the sunitinib-treated tumors ($P < .0001$; Figure 5). However, treatment with vatalanib and AMD3100 resulted in a statistically significant reduction in the tumor cell migration compared to vehicle treatment ($P < .0001$; Figure 5).

Co-expression of markers. Co-expression of CD44 (tumor cell migration), MMP-2 (infiltration), and vWF (neovascularization) in the vicinity of MHC-1–positive cells following treatment with vatalanib, sunitinib, and AMD3100 is shown in Figure 6. Under all treatment conditions, MHC-1–positive cells (green in Figure 6, *upper panel*) were at the close proximity with the areas where expression of MMP-2 was detected (red areas). However, when consecutive sections were stained for vWF and CD44 markers, not all the areas that showed MHC-1–positive cells were CD44 (red in Figure 6, lower panel) positive. In addition, except in few areas, most of the CD44-positive cells were seen to be away from vWF-positive areas. However, a few CD44-positive cells were seen in the lining of vWF-positive

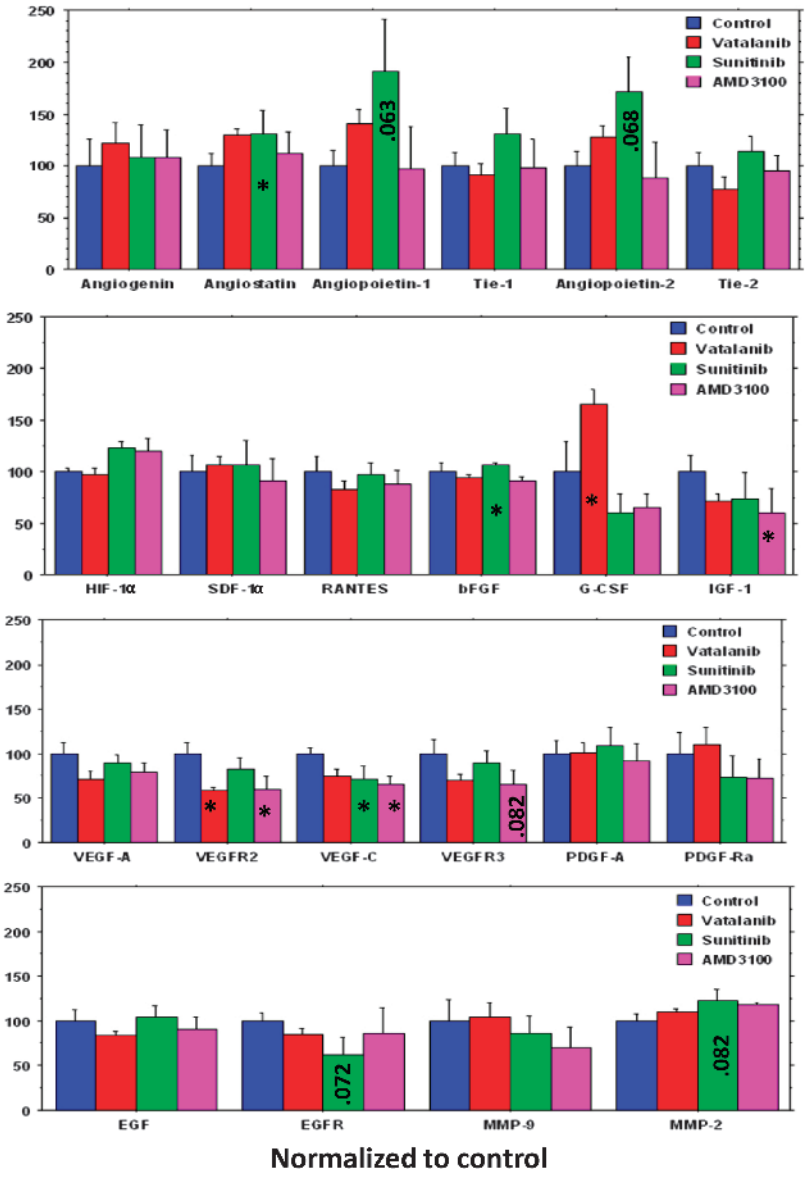

Figure 3. Quantitative analysis of tumor growth factors using protein array kit and ELISA. AMD3100 treatment resulted in a net decrease in the expression of most proangiogenic factors compared to the vehicle treatment. G-CSF expression was significantly increased after treatment with vatalanib compared to the vehicle-treated tumor. Note the significant decrease of VEGFR2 in vatalanib-treated tumors. *$P < .05$.

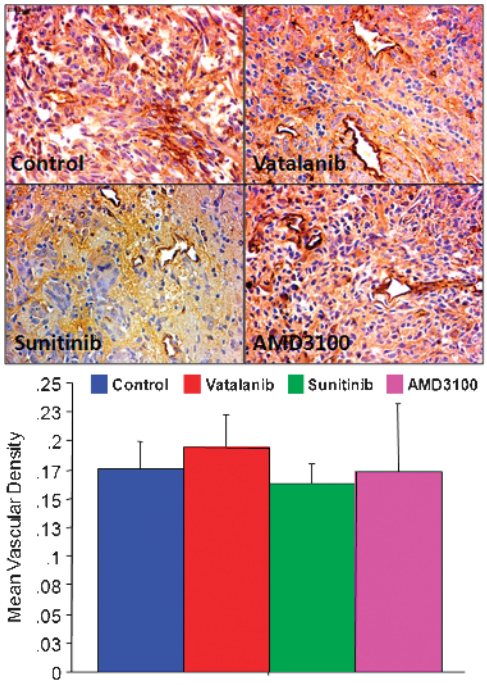

Figure 4. Histologic analysis of vascular density. Immunohistochemistry staining with anti-vWF antibody shows tumor neovascularization (upper panel; original magnification, ×40) with or without antiangiogenic treatments. Quantitative estimation of MVD by counting vWF-positive areas revealed significant changes in MVD after vatalanib, sunitinib, or AMD3100 treatments compared to the vehicle-treated tumor (lower panel). However, note the dilated and irregular vessels following treatments.

areas (yellow arrows), which may indicate the incorporation of tumor cells into neovessels.

Discussion

The interpretation of the efficacy of antiangiogenic drug treatment is currently limited by our incomplete understanding of tumor vascular physiology. Hence, it would be worthwhile to combine the available imaging and histologic techniques in understanding and predicting the efficacy of antiangiogenic therapy. The goal of this study was to determine the antiangiogenic efficacy of vatalanib, sunitinib, and AMD3100 in orthotopic U251 tumors using the dual approach. DCE-MRI was used as a noninvasive method to measure the changes in vascular parameters following antiangiogenic therapy. We also evaluated the changes in the expression of tumor factors following antiangiogenic treatment. Our results indicate that AMD3100 treatment resulted in a significant reduction of tumor growth, whereas vatalanib treatment significantly increased tumor growth as measured by MRI, which is in good agreement with our previous reports [10].

At present, conventional morphologic imaging is being used to estimate tumor response following antiangiogenic therapy. However, this technique is limited by the difficulty in distinguishing tumor- *versus* treatment-related changes. In addition, relevant clinical information can only be obtained weeks or months after treatment initiation [28]. DCE-MRI is an exciting and promising imaging tool that allows for characterization of the vascular changes by measuring specific physiological characteristics inside the tumor [29]. DCE-MRI could potentially provide clinically relevant information much earlier than the conventional imaging and would be more efficient in monitoring treatment response. AMD3100 treatment resulted in a decrease in K^{trans}, K_b, and V_e, indicating a decrease in neovascularity (permeability), interstitial space volume, and blood volume, respectively. These findings indicate a net decrease in the angiogenesis after treatment with AMD3100. Vatalanib treatment decreased whole tumor K^{trans}, K_b, and V_p but increased V_e. Although the changes were not significant compared to that of vehicle-treated tumors, the increase in V_e following drug treatment would indicate an increase in extracellular space. The increase in extracellular space may be the result of disorganization of tumor interstitial space because of neovascularization. However, presence of low level central necrosis cannot be ruled out. Sunitinib treatment nonsignificantly increased V_p that indicates an increase in tumor blood plasma volume, which could be due to increased neovascularization; however, slightly decreased K^{trans} (permeability) indicates an organized vasculature.

The expression of various tumor growth factors following antiangiogenic therapy was also evaluated. Vatalanib treatment in U251 tumors increased the expression of many proangiogenic growth factors including G-CSF, SDF-1α, angiopoietin-1 and angiopoietin-2, angiogenin, and MMP-2. The paradoxical increase in the angiogenic signal

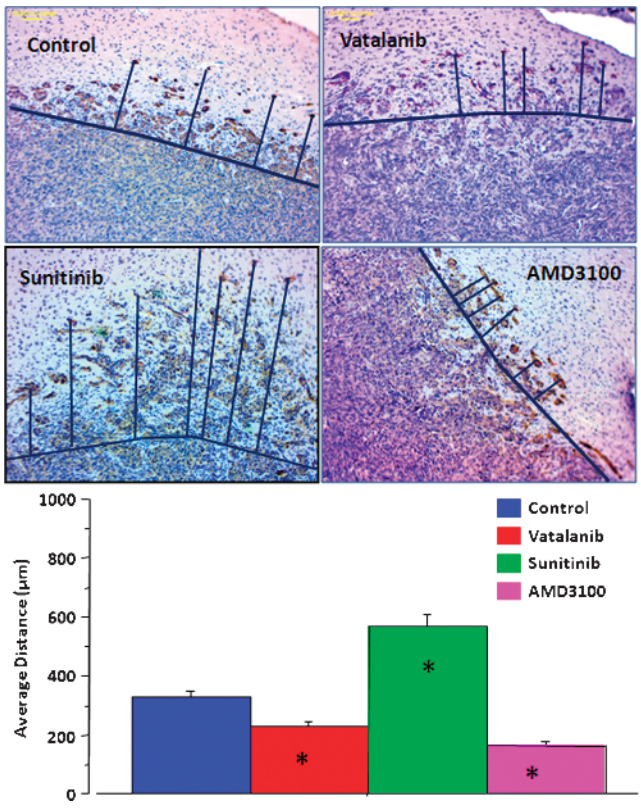

Figure 5. Migration of human marker-positive cells. Representative images of tumor sections were stained with invasion marker MHC-1 (upper panel; original magnification, ×10). The drawn lines show the margin of the primary tumor masses and the migrated tumor cells away from the margin. Sunitinib treatment resulted in a significantly increased migration of cells from the main tumor mass ($P < .0001$). Treatment with vatalanib and AMD3100 resulted in a statistically significant reduction in the tumor cell migration compared to vehicle-treated tumor ($P < .0001$) (lower panel). *$P < .05$.

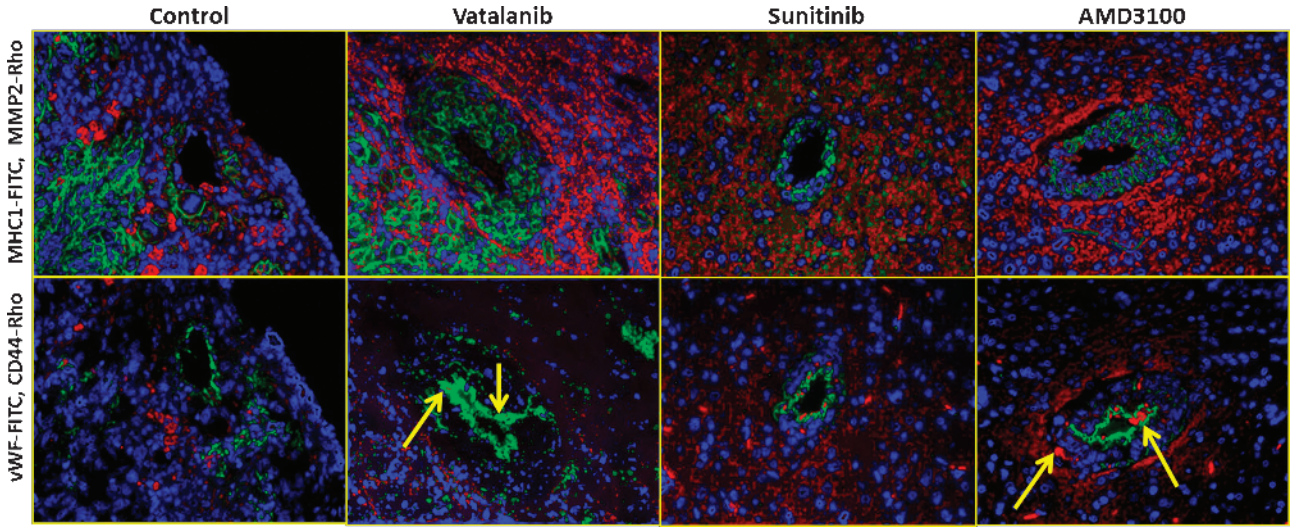

Figure 6. Co-expression of CD44, MMP-2, and vWF in the vicinity of MHC-1–positive cells, following antiangiogenic treatment. Upper panel: Double staining with anti–MHC-1 (green) and anti–MMP-2 (red) antibodies shows correlation between the two markers of tumor invasion. Lower panel: Double staining with anti-vWF (green) and anti-CD44 (red) antibodies showed CD44-positive cells lining the vWF-positive areas, indicating possible incorporation of tumor cells into new vessels (yellow arrow).

may be mediated by the alternative angiogenic pathways including SDF-1α–CXCR4 pathway and by the mobilization of BM progenitor cells due to the release of G-CSF from the tumors. G-CSF is known to be a strong mobilizer of BM cells to the peripheral blood. However, sunitinib treatment increased the expression of proangiogenic growth factors such as SDF-1α, angiopoietin-1 and angiopoietin-2, angiogenin, MMP-2, Tie-1 and Tie-2, PDGF-AA, EGF, and HIF-1α. We also observed a greater magnitude of tumor invasion as measured by the distance traveled by MHC-1–positive cells from the main tumor mass, following treatment with sunitinib. Our results are in agreement with preclinical studies that have indicated an increase in the metastatic potential of tumor cells after treatment with sunitinib [47]. AMD3100 treatment led to a decrease in the expression of most proangiogenic factors and an increase in angiostatin, an antiangiogenic protein. These changes could explain the reduction in angiogenesis and tumor growth following AMD3100 treatment. There was also a significant reduction in tumor cell invasion as seen by decreased MHC-1–positive cells away from the main tumor mass.

AMD3100 is a CXCR4 receptor antagonist and is known to inhibit SDF-1α binding to this receptor and related signal transduction [30]. The CXCR4 receptor is expressed on glioma cells and is known to play a role in their migration and invasion [31–37]. There is an experimental evidence to support the role of CXCR4/SDF-1α in glioma angiogenesis [31,37,38]. Our results indicate that the inhibition of CXCR4 receptor in gliomas could potentially lead to reduced tumor growth, angiogenesis, and invasion. Though AMD3100 reduced angiogenesis and U251 tumor growth, there was an increase in expression of some of the proangiogenic factors including MMP-2 and HIF-1α. Both MMP-2 and HIF-1α are known to promote angiogenesis through the VEGF pathway [39,40]. Our results indicate that, in addition to the VEGF pathway, CXCR4-mediated angiogenesis may also play an important role in angiogenesis and tumor growth.

Currently, there are many antiangiogenic agents under investigation in phase I/II clinical trials for the treatment of high-grade glioma [41]. Many of the novel agents have failed to show meaningful clinical benefit. Recent clinical trials using sunitinib in patients with recurrent high-grade glioma have failed to show any objective evidence of tumor control [42–44]. Similarly, vatalanib has been tested in pilot clinical trials. Although the drug was well tolerated, it was shown to have limited efficacy in a treatment of newly diagnosed GBM [45]. Though many patients demonstrate an initial clinical response to antiangiogenic therapy, no significant improvement in survival has been noted. Treatment resistance to a particular antiangiogenic drug could be mediated by non–VEGF-related angiogenesis. On the basis of our preclinical results, one of the potential targets for antiangiogenic therapy in glioma could be CXCR4 receptor–mediated vasculogenesis. Not only did CXCR4 receptor decreased tumor vascularization and growth, it also reduced tumor cell invasion and migration. In fact, AMD3100 has been previously shown to inhibit tumor growth by increasing apoptosis and decreasing proliferation in a preclinical model [46].

The study has following limitations: 1) The uniformity in the tumor size across the sample at the beginning of the treatment was not determined. However, our extensive experience in working with this model gave us sufficient information about the growth profile of the tumors. At day 7 after implantation, tumors are expected to exhibit a uniform growth and size across the sample, and the life expectancy of an untreated animal carrying tumor of this size is about 28 to 35 days after implantation [10]. 2) We did not test the expression level of proangiogenic factors in tumors before the beginning of the treatment. Tissues collected from vehicle-treated tumor-bearing animals were used as a proper indicator of the basal expression levels of proangiogenic factors in the untreated tumors.

Conclusion

In conclusion, our results indicate that AMD3100 has a significant inhibitory effect on the growth and angiogenesis in U251 tumors, as measured by MRI and protein expression levels. Vatalanib treatment paradoxically promoted angiogenesis and tumor growth in the

U251 animal model. Although sunitinib treatment resulted in inhibition of U251 tumor growth, there was no uniform inhibition of the expression of proangiogenic factors. Our results add to the growing body of evidence that implicates the importance of non–VEGF-related pathways in glioma angiogenesis and vasculogenesis. Future clinical trials are still necessary to test the antitumor efficacy of AMD3100 in the treatment of high-grade glioma.

Acknowledgments

The authors thank Tazkia Al-Bari for making MRI maps under the guidance of J.R.E.

References

[1] Los M, Roodhart JM, and Voest EE (2007). Target practice: lessons from phase III trials with bevacizumab and vatalanib in the treatment of advanced colorectal cancer. *Oncologist* **12**, 443–450.

[2] Norden AD, Young GS, Setayesh K, Muzikansky A, Klufas R, Ross GL, Ciampa AS, Ebbeling LG, Levy B, Drappatz J, et al. (2008). Bevacizumab for recurrent malignant gliomas: efficacy, toxicity, and patterns of recurrence. *Neurology* **70**, 779–787.

[3] Norden AD, Drappatz J, and Wen PY (2008). Novel anti-angiogenic therapies for malignant gliomas. *Lancet Neurol* **7**, 1152–1160.

[4] Dietrich J, Norden AD, and Wen PY (2008). Emerging antiangiogenic treatments for gliomas—efficacy and safety issues. *Curr Opin Neurol* **21**, 736–744.

[5] Oronsky BT, Knox SJ, and Scicinski JJ (2012). Is nitric oxide (NO) the last word in radiosensitization? A review. *Transl Oncol* **5**, 66–71.

[6] Miller KD, Sweeney CJ, and Sledge GW Jr (2005). Can tumor angiogenesis be inhibited without resistance? *EXS* **94**, 95–112.

[7] Thompson EM, Frenkel EP, and Neuwelt EA (2011). The paradoxical effect of bevacizumab in the therapy of malignant gliomas. *Neurology* **76**, 87–93.

[8] Grabner G, Nöbauer I, Elandt K, Kronnerwetter C, Woehrer A, Marosi C, Prayer D, Trattnig S, and Preusser M (2012). Longitudinal brain imaging of five malignant glioma patients treated with bevacizumab using susceptibility-weighted magnetic resonance imaging at 7 T. *Magn Reson Imaging* **30**, 139–147.

[9] Wong ET, Gautam S, Malchow C, Lun M, Pan E, and Brem S (2011). Bevacizumab for recurrent glioblastoma multiforme: a meta-analysis. *J Natl Compr Canc Netw* **9**, 403–407.

[10] Ali MM, Janic B, Babajani-Feremi A, Varma NR, Iskander AS, Anagli J, and Arbab AS (2010). Changes in vascular permeability and expression of different angiogenic factors following anti-angiogenic treatment in rat glioma. *PLoS One* **5**, e8727.

[11] Faivre S, Demetri G, Sargent W, and Raymond E (2007). Molecular basis for sunitinib efficacy and future clinical development. *Nat Rev Drug Discov* **6**, 734–745.

[12] Petit I, Jin D, and Rafii S (2007). The SDF-1–CXCR4 signaling pathway: a molecular hub modulating neo-angiogenesis. *Trends Immunol* **28**, 299–307.

[13] Kioi M, Vogel H, Schultz G, Hoffman RM, Harsh GR, and Brown JM (2010). Inhibition of vasculogenesis, but not angiogenesis, prevents the recurrence of glioblastoma after irradiation in mice. *J Clin Invest* **120**, 694–705.

[14] Esmaeili M, Bathen TF, Engebråten O, Maelandsmo GM, Gribbestad IS, and Moestue SA (2013). Quantitative ^{31}P HR-MAS MR spectroscopy for detection of response to PI3K/mTOR inhibition in breast cancer xenografts. *Magn Reson Med.* DOI: 10.1002/mrm.24869 [Epub ahead of print 22 July].

[15] Taylor JS, Tofts PS, Port R, Evelhoch JL, Knopp M, Reddick WE, Runge VM, and Mayr N (1999). MR imaging of tumor microcirculation: promise for the new millennium. *J Magn Reson Imaging* **10**, 903–907.

[16] Knopp MV, Weiss E, Sinn HP, Mattern J, Junkermann H, Radeleff J, Magener A, Brix G, Delorme S, Zuna I, et al. (1999). Pathophysiologic basis of contrast enhancement in breast tumors. *J Magn Reson Imaging* **10**, 260–266.

[17] Bagher-Ebadian H, Jain R, Nejad-Davarani SP, Mikkelsen T, Lu M, Jiang Q, Scarpace L, Arbab AS, Narang J, Soltanian-Zadeh H, et al. (2012). Model selection for DCE-T1 studies in glioblastoma. *Magn Reson Med* **68**, 241–251.

[18] Ewing JR, Brown SL, Lu M, Panda S, Ding G, Knight RA, Cao Y, Jiang Q, Nagaraja TN, Churchman JL, et al. (2006). Model selection in magnetic resonance imaging measurements of vascular permeability: Gadomer in a 9L model of rat cerebral tumor. *J Cereb Blood Flow Metab* **26**, 310–320.

[19] Janic B and Arbab AS (2012). Cord blood endothelial progenitor cells as therapeutic and imaging probes. *Imaging Med* **4**, 477–490.

[20] Kumar S, Arbab AS, Jain R, Kim J, Decarvalho AC, Shankar A, Mikkelsen T, and Brown SL (2012). Development of a novel animal model to differentiate radiation necrosis from tumor recurrence. *J Neurooncol* **108**, 411–420.

[21] McGowan PM, Simedrea C, Ribot EJ, Foster PJ, Palmieri D, Steeg PS, Allan AL, and Chambers AF (2011). Notch1 inhibition alters the CD44^{hi}/CD24^{lo} population and reduces the formation of brain metastases from breast cancer. *Mol Cancer Res* **9**, 834–844.

[22] Gutova M, Najbauer J, Gevorgyan A, Metz MZ, Weng Y, Shih CC, and Aboody KS (2007). Identification of uPAR-positive chemoresistant cells in small cell lung cancer. *PLoS One* **2**, e243.

[23] Yoshida T, Matsuda Y, Naito Z, and Ishiwata T (2012). CD44 in human glioma correlates with histopathological grade and cell migration. *Pathol Int* **62**, 463–470.

[24] Arbab AS, Thiffault C, Navia B, Victor SJ, Hong K, Zhang L, Jiang Q, Varma NR, Iskander A, and Chopp M (2012). Tracking of In-111-labeled human umbilical tissue-derived cells (hUTC) in a rat model of cerebral ischemia using SPECT imaging. *BMC Med Imaging* **12**, 33.

[25] Zhang L, Li Y, Zhang C, Chopp M, Gosiewska A, and Hong K (2011). Delayed administration of human umbilical tissue-derived cells improved neurological functional recovery in a rodent model of focal ischemia. *Stroke* **42**, 1437–1444.

[26] Christensen K, Aaberg-Jessen C, Andersen C, Goplen D, Bjerkvig R, and Kristensen BW (2010). Immunohistochemical expression of stem cell, endothelial cell, and chemosensitivity markers in primary glioma spheroids cultured in serum-containing and serum-free medium. *Neurosurgery* **66**, 933–947.

[27] Weidner N, Semple JP, Welch WR, and Folkman J (1991). Tumor angiogenesis and metastasis—correlation in invasive breast carcinoma. *N Engl J Med* **324**, 1–8.

[28] Levin VA, Bidaut L, Hou P, Kumar AJ, Wefel JS, Bekele BN, Prabhu S, Loghin M, Gilbert MR, and Jackson EF (2011). Randomized double-blind placebo-controlled trial of bevacizumab therapy for radiation necrosis of the central nervous system. *Int J Radiat Oncol Biol Phys* **79**, 1487–1495.

[29] Ewing JR, Knight RA, Nagaraja TN, Yee JS, Nagesh V, Whitton PA, Li L, and Fenstermacher JD (2003). Patlak plots of Gd-DTPA MRI data yield blood-brain transfer constants concordant with those of ^{14}C-sucrose in areas of blood-brain opening. *Magn Reson Med* **50**, 283–292.

[30] Donzella GA, Schols D, Lin SW, Esté JA, Nagashima KA, Maddon PJ, Allaway GP, Sakmar TP, Henson G, De Clercq E, et al. (1998). AMD3100, a small molecule inhibitor of HIV-1 entry via the CXCR4 co-receptor. *Nat Med* **4**, 72–77.

[31] Rempel SA, Dudas S, Ge S, and Gutiérrez JA (2000). Identification and localization of the cytokine SDF1 and its receptor, CXC chemokine receptor 4, to regions of necrosis and angiogenesis in human glioblastoma. *Clin Cancer Res* **6**, 102–111.

[32] Oh JW, Drabik K, Kutsch O, Choi C, Tousson A, and Benveniste EN (2001). CXC chemokine receptor 4 expression and function in human astroglioma cells. *J Immunol* **166**, 2695–2704.

[33] Ehtesham M, Winston JA, Kabos P, and Thompson RC (2006). CXCR4 expression mediates glioma cell invasiveness. *Oncogene* **25**, 2801–2806.

[34] Hong X, Jiang F, Kalkanis SN, Zhang ZG, Zhang XP, DeCarvalho AC, Katakowski M, Bobbitt K, Mikkelsen T, and Chopp M (2006). SDF-1 and CXCR4 are up-regulated by VEGF and contribute to glioma cell invasion. *Cancer Lett* **236**, 39–45.

[35] Woerner BM, Warrington NM, Kung AL, Perry A, and Rubin JB (2005). Widespread CXCR4 activation in astrocytomas revealed by phospho-CXCR4-specific antibodies. *Cancer Res* **65**, 11392–11399.

[36] Zhou Y, Larsen PH, Hao C, and Yong VW (2002). CXCR4 is a major chemokine receptor on glioma cells and mediates their survival. *J Biol Chem* **277**, 49481–49487.

[37] Zagzag D, Lukyanov Y, Lan L, Ali MA, Esencay M, Mendez O, Yee H, Voura EB, and Newcomb EW (2006). Hypoxia-inducible factor 1 and VEGF upregulate CXCR4 in glioblastoma: implications for angiogenesis and glioma cell invasion. *Lab Invest* **86**, 1221–1232.

[38] Yang SX, Chen JH, Jiang XF, Wang QL, Chen ZQ, Zhao W, Feng YH, Xin R, Shi JQ, and Bian XW (2005). Activation of chemokine receptor CXCR4 in malignant glioma cells promotes the production of vascular endothelial growth factor. *Biochem Biophys Res Commun* **335**, 523–528.

[39] Munaut C, Nöel A, Hougrand O, Foidart JM, Boniver J, and Deprez M (2003). Vascular endothelial growth factor expression correlates with matrix

metalloproteinases MT1-MMP, MMP-2 and MMP-9 in human glioblastomas. *Int J Cancer* **106**, 848–855.

[40] Maxwell PH, Dachs GU, Gleadle JM, Nicholls LG, Harris AL, Stratford IJ, Hankinson O, Pugh CW, and Ratcliffe PJ (1997). Hypoxia-inducible factor-1 modulates gene expression in solid tumors and influences both angiogenesis and tumor growth. *Proc Natl Acad Sci USA* **94**, 8104–8109.

[41] Taylor J and Gerstner ER (2013). Anti-angiogenic therapy in high-grade glioma (treatment and toxicity). *Curr Treat Options Neurol* **15**, 328–337.

[42] Neyns B, Sadones J, Chaskis C, Dujardin M, Everaert H, Lv S, Duerinck J, Tynninen O, Nupponen N, Michotte A, et al. (2011). Phase II study of sunitinib malate in patients with recurrent high-grade glioma. *J Neurooncol* **103**, 491–501.

[43] Reardon DA, Vredenburgh JJ, Coan A, Desjardins A, Peters KB, Gururangan S, Sathornsumetee S, Rich JN, Herndon JE, and Friedman HS (2011). Phase I study of sunitinib and irinotecan for patients with recurrent malignant glioma. *J Neurooncol* **105**, 621–627.

[44] Pan E, Yu D, Yue B, Potthast L, Chowdhary S, Smith P, and Chamberlain M (2012). A prospective phase II single-institution trial of sunitinib for recurrent malignant glioma. *J Neurooncol* **110**, 111–118.

[45] Brandes AA, Stupp R, Hau P, Lacombe D, Gorlia T, Tosoni A, Mirimanoff RO, Kros JM, and van den Bent MJ (2010). EORTC study 26041-22041: phase I/II study on concomitant and adjuvant temozolomide (TMZ) and radiotherapy (RT) with PTK787/ZK222584 (PTK/ZK) in newly diagnosed glioblastoma. *Eur J Cancer* **46**, 348–354.

[46] Rubin JB, Kung AL, Klein RS, Chan JA, Sun Y, Schmidt K, Kieran MW, Luster AD, and Segal RA (2003). A small-molecule antagonist of CXCR4 inhibits intracranial growth of primary brain tumors. *Proc Natl Acad Sci USA* **100**, 13513–13518.

[47] Welti JC, Powles T, Foo S, Gourlaouen M, Preece N, Foster J, Frentzas S, Bird D, Sharpe K, van Weverwijk A, et al. (2012). Contrasting effects of sunitinib within *in vivo* models of metastasis. *Angiogenesis* **15**, 623–641.